Energy & Environmental Science

Accepted Manuscript

ROYAL SOCIETY OF CHEMISTRY

www.rsc.org/ees

Energy &Environmental Science

COMMUNICATION

Nitrogen-doped Activated Carbon for High Energy Hybrid Supercapacitor

Received 00th January 20xx,
Accepted 00th January 20xx

DOI: 10.1039/x0xx00000x

www.rsc.org/

Bing Li,[a,†] Fang Dai,[b,†] Qiangfeng Xiao,[b] Li Yang,[b] Jingmei Shen,[c] Cunman Zhang,[a,*] and Mei Cai[b,*]

Nitrogen-doped activated carbons (NACs) were prepared through a one-step process. The obtained NACs show high surface area up to 2900 m^2g^{-1} with a moderate N content up to 4 wt%. Electrochemical evaluation of the NACs show a high specific capacity of 129 $mAhg^{-1}$ (185 Fg^{-1}) in organic electrolyte at a current density of 0.4 Ag^{-1}, as well as excellent rate capability and cycling stability. The hybrid-type supercapacitor assembled using the NACs and Si/C electrode exhibites a high material level energy density of 230 $Whkg^{-1}$ at 1747 Wkg^{-1}. The hybrid device achieved 76.3% capacity retention after 8000 cycles tested at 1.6 Ag^{-1}.

In recent years, rapid growing commercial electrical device market evokes high demand of novel energy storage systems that can provide higher energy and power than traditional systems.[1,2] Besides lithium-ion batteries, supercapacitor has been recognized as promising system for power-based applications. Comparing with traditional dielectric capacitors, supercapacitors can provide higher energy density while maintaining the high power output.[3] However, although providing extremely long cycling life, their relatively low energy-to-power ratio hindered their further application in some area where both energy and power are required, such as hybrid electrical vehicles (HEV). In order to further improve the performance, novel capacitor systems utilizing different surface chemistry and device configuration has been proposed and investigated. Recently, hybrid-type supercapacitors (HS), or called supercapacitor-battery hybrid system, attracted attention due to their high energy/power ratio, comparing with traditional electron double-layer capacitors (EDLC). Such systems utilize traditional capacitor electrode as one electrode via sorption of ions, and lithium-ion battery (LIB) electrode as counter electrode via Li ion insertion/intercalation.[4,5] The application of promising high energy LIB electrode materials help improve the performance of the hybrid system significantly. Several examples have been reported with exciting results.[6–10] Among those, the configuration using high energy LIB anode materials, such as silicon, could provide higher energy density and power density.[8] However, the energy and power density of the device are determined by the cathode part due to the asymmetrical configuration and huge difference in specific capacity of cathode and anode. Therefore, a further improvement of the system level performance is still prohibited by the cathode materials, which always have much lower specific capacity (or capacitance) than those of anode materials.[1] The same issue has been emphasized in the LIB studies.[11,12] Thus, development on cathode material for the HS with improved electrochemical performance is highly necessary.

Activated carbons (ACs) have been widely used as active material in many types of supercapacitors, due to their high surface area and porous structure which are important to final power and energy storage capacity.[4,13,14] Other advantages such as low cost and industrial large-scale production which are also superior to other types of porous materials, are critical for their application in commercial capacitor devices, too.[14] Unfortunately, common physical or chemical activation methods always produce a wide range of pore size distribution, ranging from micro-size to macro-size.[15] The specific capacitance of such kind of ACs is thus limited, although having high surface area up to 3000 m^2g^{-1}. Therefore novel activation or preparation methods providing narrow pore size distribution and controllable pore structure is necessary for further development of AC materials.

Besides structure tuning, proper surface functionality also help improve the performance of AC materials. Recently, nitrogen-doping was found help increase the specific capacitance of AC materials effectively.[16–20] Possible explanations for the capacitance increase are the faradaic reaction of the nitrogen-containing functional groups and improving wettability of the pore walls. Some recent research

[a] Clean Energy Automotive Engineering Center & School of Automotive Studies, 4800 Caoan Road, Tongji University (Jiading Campus), Shanghai 201804, China. zhangcunman@tongji.edu.cn
[b] General Motors R&D center, Warren, MI 48090, United States. mei.cai@gm.com
[c] Optimal CAE, Plymouth, MI 48170, United states
† These authors contributed equally to this work

Electronic Supplementary Information (ESI) available: [details of any supplementary information available should be included here]. See DOI: 10.1039/x0xx00000x

results also suggest that the heteroatom doping can increase the conductivity of porous carbon materials.[21–24]

Herein we report a novel one-step process for nitrogen-dope ACs (NACs) preparation utilizing agricultural waste (corncob) as precursor. The obtained NACs had a narrow micro- to meso- pore distribution and showed a high specific surface area of up to 2859 m^2g^{-1} with a moderate N content of up to 4 wt%. The NACs delivered a high specific capacity of up to 129 $mAhg^{-1}$ (185 Fg^{-1}) in organic electrolyte at a current density of 0.4 Ag^{-1}, as well as an excellent rate capability and much improve cycle stability. The HS assembled using the NACs and Si/C electrode materials showed an energy density of 230 $Whkg^{-1}$ at power density of 1747 Wkg^{-1}. Even at elevated working power density of 30127 Wkg^{-1}, such a supercapacitor can still provide an energy density of 141 $Whkg^{-1}$. To our knowledge, this is the highest value among previously reported literature results. Such HS device also showed a good cycling stability with 76.3% capacity retention after 8000 cycles at 1.6 Ag^{-1}.

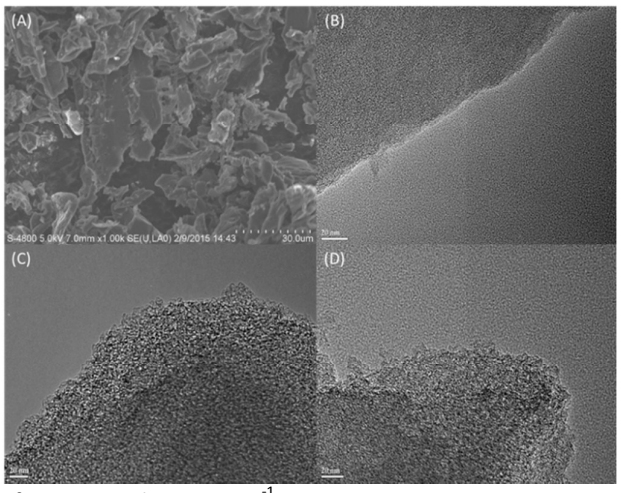

Figure 1 (A) SEM image of NAC-400, TEM image of (B) NAC-0, (C) NAC-400, and (D) NAC-600.

Results and discussion

Synthesis

In this work, corncobs were utilized as the precursor for NACs preparation. The corncobs were pre-dried at 120 °C for 12 hours before being grounded and sieved. The powders were mixed with KOH followed by heat treatment at different temperature under N_2 flow with NH3 as nitrogen source. Three NACs, namely NAC-x where x is the heat treatment temperature, were prepared and used for further characterization and electrochemical performance evaluation.

Characterizations

The bulk particle of NACs is micron-sized ranging from 5 to 30 µm, as shown in Figure 1A and Figure S1. There was no observable macro-sized pore and large meso-sized pore based on the TEM images of all NACs shown in Figure 1 B-D. Nitrogen content of all samples were determined by elemental analysis. As the heat treatment temperature increases, the nitrogen content increases form 2.97 wt% for NAC-400 to 3.98 wt% for NAC-600. Oxygen content was also found accompanied with nitrogen. NAC-400 shows oxygen content of 9.8 wt%, while NAC-600 had oxygen content of 9.05 wt%. All NACs show similar C and O signals (C1s, O1s) in XPS spectra (Figure 2A, Figure S2). Typical C1s, O1s and N1s of the synthesized carbon (NAC-400) are shown in Figure 2 A. The C1s peak is dominated by C-C bond (diamond and graphite type) at 248.8 eV. Small amount ethereal carbon (C-OH, 286 eV) and carbonyl carbon (C=O, 290 eV) can also be detected from both the C1s and O1s XPS (531.5 eV and 532.5 eV).[25,26] This type of surface functional groups is well known to increase the capacity of the engineered carbon for their fast reaction with lithium.[27] The N1s peak is mainly composed of pyridinic N (399.7 eV), together with small amount of N-oxides (402 eV).[14,28,29] In contrast, the NAC-600 has two peaks in the same range instead of one, as shown in Figure S2. The contribution from N-oxides was more than that of NAC-400. Raman spectra of NACs show intensive G bands, suggesting partially graphication of all activated carbon materials (Figure 2B).[30] With higher heat treatment temperature, much more graphication is obtained for NAC materials, as shown in Figure 2B.

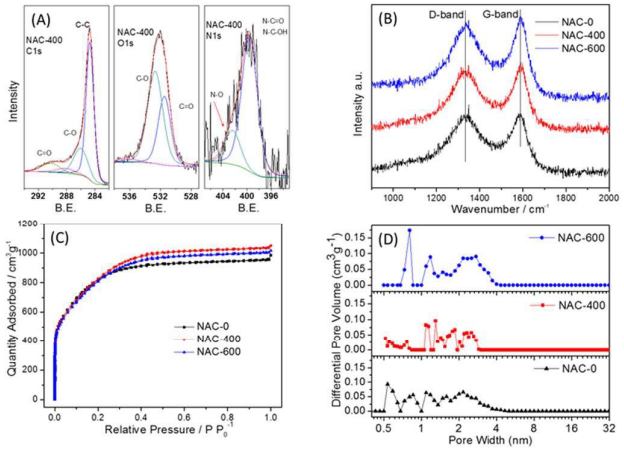

Figure 2 (A) XPS spectra of NAC-400, (B) Raman spectra of all NACs, (C) nitrogen adsorption isotherms at 77K, and (D) pore-size distribution of NACs.

The pore structure of NACs was analyzed by N2-sorption at 77K. The isotherms plots in Figure 2C clearly show type I isotherm curves with well-defined plateaus, suggesting a microporous nature of the NACs. The pore size distributions were calculated by Density Functional Theory (DFT) method and were shown in Figure 2D. All samples have pore distribution peaks between 0.5 and 5 nm, which suggests the formation of both micropores and small mesopores. As the heat treatment temperature increases, the pore size distribution peaks at mesopore range become broader, suggesting formation of slightly larger size mesopores. All NACs show similar high BET specific surface area of 2759, 2859 and 2787 m^2g^{-1} for NAC-0, NAC-400 and NAC-600, respectively.

Electrochemical performance

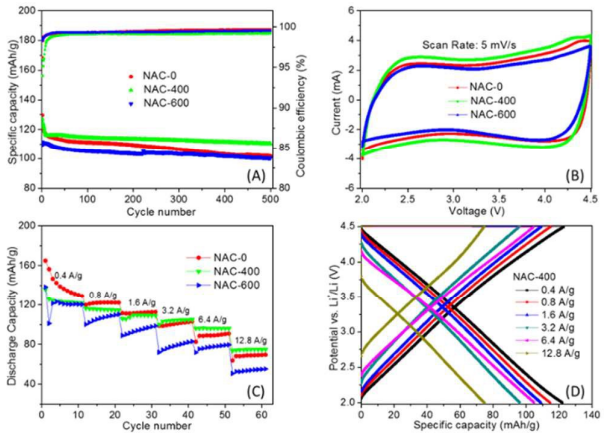

Figure 3 (A) Cycling performance of all NACs, (B) CV diagram of all NACs at scan rate of 5 mV/s, (C) rate performance of all NACs, and (D) Voltage profile of NAC-400 at different current densities.

The electrochemical performance of NACs were evaluated using coin format cell. The capacities were read from the instrument by galvanostatic charge/discharge method. Corresponding specific capacitance was calculated based on the capacity (see supporting information). Figure 3A shows the cycling performance of all NAC materials at current density of 0.4 Ag^{-1}. Both NAC-0 and NAC-400 show high initial specific capacity of 129 $mAhg^{-1}$ (185 Fg^{-1}) and 127 $mAhg^{-1}$ (182 Fg^{-1}), respectively. In contrast, the NAC-600 has lower initial capacity of 110 $mAhg^{-1}$. All NAC materials show good cycling stability and Coulombic efficiency (CE). NAC-400 shows the best capacity retention of about 86% (110 $mAhg^{-1}$) after 500 cycles among all samples. The cycling CE is above 99.2% after initial cycles. The Cyclic voltammetry (CV) profiles of NACs maintain quasi-rectangular shape at 5 mV/s scan rate, indicating the capacitive behavior of all samples (Figure 3B). Figure 3C shows the performance of NAC materials under varies current densities. The difference in specific capacities of all samples becomes more and more distinct with increased current density. At low current densities of 0.4 Ag^{-1}, all three NACs show similar specific capacity at above 110 $mAhg^{-1}$. However, at elevated current density of 0.8 Ag^{-1} and 1.6 Ag^{-1}, the specific capacity of NAC-600 drops significantly lower than the other two materials. At a high current density of 12.8 Ag^{-1} (128 C), the NAC-400 provides a capacity of 73.7 $mAhg^{-1}$, which is 15% and 33% higher than those of NAC-0 (63.8 $mAhg^{-1}$) and NAC-600 (55.3 $mAhg^{-1}$).

The electrochemical performance of the NAC materials is considered depending on the N-doping of the materials. Both the specific capacity and cycling stability were improved by increasing the N amount from 0 wt% of NAC-0 to 2.97 wt% of NAC-400. However, when the N-doping further increased to 3.98 wt% for NAC-600, the electrochemical performance including reversible capacity, capacity retention, and rate performance become worse comparing with those of NAC-400. The much increased oxidized pyridinic N found in NAC-600 is considered as one key factor resulting in capacity drop due to the positive charge on N which will affect the ion adsorption.20 A slightly reduced BET surface area of NAC-600 also affect the specific capacity drop.

The N-doping of NACs also help improve the conductivity, as supported by electrochemical impedance spectroscopy (EIS) (Figure S3). In particular, the diameter of the kinetic loop corresponds to charge transfer resistance of the NAC-400, which has a strong impact on the specific capacity, was much smaller than that of the NAC-0. The linear galvanostatic charge/discharge profiles of NAC-400 were tested at 0.4 - 12.8 Ag^{-1}, meaning capacitive behavior with the adsorption/desorption of ions on the electrode surface, as shown in Figure 3D.

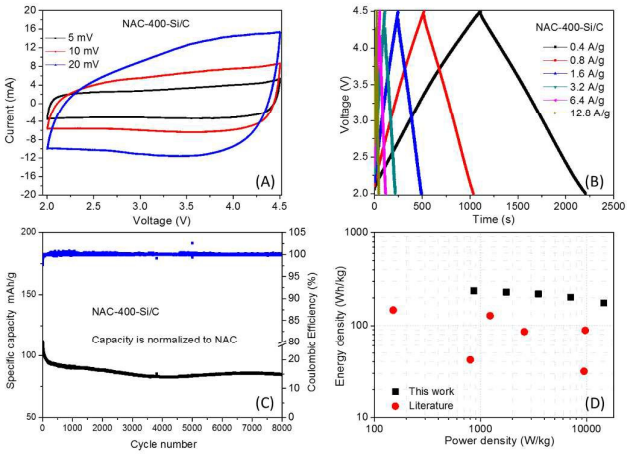

Figure 4. (A) CV diagram of NAC-400-Si/C HS full cell at different scan rate, (B) voltage profile of NAC-400-Si/C HS, (C) long cycling performance of NAC-400-Si/C HS at 0.4 Ag^{-1}, specific capacity is normalized to NAC-400, and (D) Ragone plot of the NAC-400-Si/C HS.

HS full cell was assembled using NAC-400 as the cathode and Si/C as the anode materials (see supporting information). During the charge process, PF^-_6 were absorbed in the porous structure of NAC, while Li^+ from electrolyte were alloyed with the Si/C. Discharge process was in reverse of the charge process. Mass ratio of the electrode active materials was optimized to 2:1 for the best electrochemical performance and energy/power density (see supporting information).

The CV profile of the HS showed a gradual deviation from the ideal rectangular shape with increasing scan rate, which is owing to the overlapping effects of two different energy-storage mechanisms (Figure 4A). This observation is consistent with the voltage profile of the HS using galvanostatic charge/discharge method, which showed little deviation from the linear slop (Figure 4B). The HS showed good cycling stability of 76.3% capacity retention in 8000 cycles at a high current density of 1.6 Ag^{-1} (Figure 4C). The Coulombic efficiency of the full cell is relative high, with an average of 99.8 %. The Ragone plot (power density vs. energy density, material level) of HS is shown in Figure 4D. The energy density and power density were calculated based on the total mass of active materials on both the cathode and the anode. The detailed calculation method of the energy and power density is in supporting information. The HS showed a high energy density of 230 $Whkg^{-1}$ at 1747 Wkg^{-1}, which also remains of

141 Whkg^{-1} even when power density elevated to 30127 Wkg^{-1}. Table S2 listed some Li-ion hybrid systems with typical energy and power densities for an approximate comparison, such as AC//hard carbon[31], AC//soft carbon[32], AC//LTO[33], AC//B-Si/SiO2/C[8], 3D graphene//Fe3O4/graphene[7], CNS//MnO/CNS[9], as well as an example of Na-ion hybrid system PSNC//PSOC-A[34]. The performance of this work is still quite promising and is among the best reported hybrid type of supercapacitors.

We also found that a narrower voltage window help increase the long cycling stability, although sacrificing the energy density. When the voltage window changes to 2 - 4.0 V, energy density reduces 30% at the same power density, while the cycling performance improved with a capacity retention of 88% after 8000 cycles (Figure S4 and Table S1).

Conclusions

In summary, novel N-doped activated carbons were synthesized via one-step method. The obtained NACs showed excellent electrochemical performance with a specific capacity up to 129 mAhg^{-1} and capacity retention of 86% in 500 cycles. The N-doping of the NACs was found to help improving the performance. The Hybrid-type supercapacitor was further assembled and evaluated utilizing NACs and Si/C nanocomposite. With the optimized N/P ratio, the hybrid system showed a high energy densities of 230 – 141 Whkg^{-1} at power density from 1747 to 30127 Wkg^{-1}, which are among the highest numbers of reported hybrid-type systems. Good long cycling stability was also obtained with a capacity retention of 76.3 % after 8000 cycles for the hybrid-type supercapacitor.

Acknowledgements

The authors appreciate General motors project (Project No. 1550) and International Postdoctoral Exchange Fellowship Program China (201372) for the financial support. We also thank Dr. Peng Lu (General Motors) for his help with XPS analysis.

References

1 G. Wang, L. Zhang and J. Zhang, Chem. Soc. Rev., 2012, 41, 797–828.
2 M. Armand and J.-M. Tarascon, Nature, 2008, 451, 652–657.
3 P. Sharma and T. S. Bhatti, Energy Convers. Manag., 2010, 51, 2901–2912.
4 Y. Wang and Y. Xia, Adv. Mater., 2013, 25, 5336–5342.
5 G. G. Amatucci, F. Badway, A. Du Pasquier and T. Zheng, J. Electrochem. Soc., 2001, 148, A930.
6 Q. Wang, Z. H. Wen and J. H. Li, Adv. Funct. Mater., 2006, 16, 2141–2146.
7 F. Zhang, T. Zhang, X. Yang, L. Zhang, K. Leng, Y. Huang and Y. Chen, Energy Environ. Sci., 2013, 6, 1623–1632.
8 R. Yi, S. Chen, J. Song, M. L. Gordin, A. Manivannan and D. Wang, Adv. Funct. Mater., 2014, 24, 7433–7439.
9 H. Wang, Z. Xu, Z. Li, K. Cui, J. Ding, A. Kohandehghan, X. Tan, B. Zahiri, B. C. Olsen, C. M. B. Holt and D. Mitlin, Nano Lett., 2014, 14, 1987–1994.
10 K. Leng, F. Zhang, L. Zhang, T. Zhang, Y. Wu, Y. Lu, Y. Huang and Y. Chen, Nano Res., 2013, 6, 581–592.
11 M. S. Whittingham, Chem. Rev., 2004, 104, 4271–4302.
12 J. B. Goodenough and Y. Kim, Chem. Mater., 2010, 22, 587–603.
13 L. L. Zhang and X. S. Zhao, Chem. Soc. Rev., 2009, 38, 2520–2531.
14 A. G. Pandolfo and A. F. Hollenkamp, J. Power Sources, 2006, 157, 11–27.
15 M. Inagaki, H. Konno and O. Tanaike, J. Power Sources, 2010, 195, 7880–7903.
16 J. Lee, J. Kim and T. Hyeon, Adv. Mater., 2006, 18, 2073–2094.
17 G. Lota, B. Grzyb, H. Machnikowska, J. Machnikowski and E. Frackowiak, Chem. Phys. Lett., 2005, 404, 53–58.
18 H. Guo and Q. Gao, J. Power Sources, 2009, 186, 551–556.
19 K. Jurewicz, K. Babeł, A. Źiółkowski and H. Wachowska, Electrochim. Acta, 2003, 48, 1491–1498.
20 M. Seredych, D. Hulicova-Jurcakova, G. Q. Lu and T. J. Bandosz, Carbon N. Y., 2008, 46, 1475–1488.
21 E. Raymundo-Piñero, M. Cadek and F. Béguin, Adv. Funct. Mater., 2009, 19, 1032–1039.
22 F. Béguin, K. Szostak, G. Lota and E. Frackowiak, Adv. Mater., 2005, 17, 2380–2384.
23 H. M. Jeong, J. W. Lee, W. H. Shin, Y. J. Choi, H. J. Shin, J. K. Kang and J. W. Choi, Nano Lett., 2011, 11, 2472–2477.
24 Y. Chen, X. Zhang, D. Zhang, P. Yu and Y. Ma, Carbon N. Y., 2011, 49, 573–580.
25 Z. Li, Z. Xu, H. Wang, J. Ding, B. Zahiri, C. M. B. Holt, X. Tan and D. Mitlin, Energy Environ. Sci., 2014, 7, 1708.
26 C.-M. Chen, Q. Zhang, M.-G. Yang, C.-H. Huang, Y.-G. Yang and M.-Z. Wang, Carbon N. Y., 2012, 50, 3572–3584.
27 Z. Li, Z. Xu, X. Tan, H. Wang, C. M. B. Holt, T. Stephenson, B. C. Olsen and D. Mitlin, Energy Environ. Sci., 2013, 6, 871.
28 C. O. Ania, V. Khomenko, E. Raymundo-Piñero, J. B. Parra and F. Béguin, Adv. Funct. Mater., 2007, 17, 1828–1836.
29 S. Biniak, G. Szymański, J. Siedlewski and A. Świątkowski, Carbon N. Y., 1997, 35, 1799–1810.
30 Y. Wang, D. C. Alsmeyer and R. L. McCreery, Chem. Mater., 1990, 2, 557–563.
31. J.-H. Kim, J.-S. Kim, Y.-G. Lim, J.-G. Lee and Y.-J. Kim, J. Power Sources, 2011, 196, 10490–10495.
32. M. Schroeder, M. Winter, S. Passerini and A. Balducci, J. Power Sources, 2013, 238, 388–394.
33. A. Jain, V. Aravindan, S. Jayaraman, P. S. Kumar, R. Balasubramanian, S. Ramakrishna, S. Madhavi and M. P. Srinivasan, Sci. Rep., 2013, 3, 3002.
34. J. Ding, H. Wang, Z. Li, K. Cui, D. Karpuzov, X. Tan, A. Kohandehghan and D. Mitlin, Energy Environ. Sci., 2015, 8, 941–955.

Broader Context

The present work provide a novel one-step synthesis for nitrogen-doped activated carbon. The excellent performance of the N-doped AC allows their further application in hybrid-type supercapacitor, which utilizes a combination of the capacitor electrode and Li-ion battery anode. The special configuration can much improve the energy density, which could be several times of traditional electric double-layer supercapacitor, without sacrificing the power density. The N-doped AC and corresponding hybrid supercapacitor presenting in this work can provide a good example for novel material and system design for advanced energy storage system